1-1-2010

Decoherence by electromagnetic fluctuations in double-quantum-dot charge qubits

Diego C. B. Valente

Eduardo R. Mucciolo
University of Central Florida

F. K. Wilhelm

Decoherence by electromagnetic fluctuations in double-quantum-dot charge qubits

Diego C. B. Valente,[1] Eduardo R. Mucciolo,[2] and F. K. Wilhelm[3]
[1]*Department of Physics, University of Connecticut, Storrs, Connecticut 06269, USA*
[2]*Department of Physics, University of Central Florida, Orlando, Florida 32816-2385, USA*
[3]*Institute of Quantum Computation, Department of Physics and Astronomy, University of Waterloo, Waterloo, Ontario, Canada N2L 3G1*
(Received 5 May 2010; published 3 September 2010)

We discuss decoherence due to electromagnetic fluctuations in charge qubits formed by two lateral quantum dots. We use effective circuit model to evaluate correlations of voltage fluctuations in the qubit setup. These correlations allows us to estimate energy (T_1) and phase (T_2) relaxation times of the qubit system. Our theoretical estimate of the quality factor due to dephasing by electromagnetic fluctuations yields values much higher than those found in recent experiments, indicating that other sources of decoherence play a dominant role.

DOI: 10.1103/PhysRevB.82.125302 PACS number(s): 73.21.La, 03.67.Lx, 73.23.Hk

I. INTRODUCTION

Solid-state semiconductor lateral quantum dots are strong candidates for the physical realization of qubits. These artificial systems can be designed to allow for the observation of coherent oscillations between their quantum states. Since its first proposals,[1,2] a wide variety of experiments have demonstrated control over the spin degree of freedom of confined electrons in quantum dots,[3,4] as well as charge states.[5–8] Solid-state quantum computer architectures with qubits encoded in dopant atoms in semiconductor crystals have also been proposed.[9] Quantum dots present the ubiquitous advantages of being manufactured from highly developed semiconductor technology and may offer easier scalability, the latter being key in enabling the manufacturing of large-scale quantum computers in the future. A drawback to their use in quantum computers is that they also couple rather effectively to external degrees of freedom which lead to decoherence.

Semiconductor qubits are susceptible to various decoherence mechanisms. Hyperfine coupling to lattice nuclear spins reduces the phase coherence of electron spins[10,11] while qubits based on the charge degree of freedom are particularly sensitive to decoherence mechanisms related to charge motion, such as coupling to phonon modes and to charge traps in the substrate. Several of these sources have been investigated.[12–21]

In this paper we focus on charge-based qubits. The simplest realization of a charge qubit is a double-quantum-dot (DQD) system with an odd number of electrons, as shown schematically in Fig. 1. So far measurements of quality (Q) factors of coherent oscillations in these systems have yielded rather low values in the range of 3–9.[6–8] In an effort to identify the main sources of decoherence, theoretical estimates of the Q factor have been carried out assuming mainly the coupling to acoustic phonons.[12–21] However, a discrepancy of at least one order of magnitude remains between the experimental value and the theoretical estimates, with the latter predicting larger Q factors. This discrepancy indicates that the phonons may not be the dominant noise source in current experimental setups. Thus, an investigation of other possible environmental decoherence mechanisms is in order. Here, we consider the coupling of the DQD charge-based qubit systems to voltage fluctuations in the gates.

This paper is organized as follows. In Sec. II we define the DQD effective Hamiltonian and the interaction between the qubit and the gate-voltage fluctuations. In Sec. III we introduce the effective circuit model that describes the DQD and the electromagnetic environment, as well as the Hamiltonian of the latter. In Sec. V we estimate the equivalent circuit parameters and in Sec. VI we calculate upper bounds to the decoherence rates and Q factors. Our main finding is that voltage fluctuations cause only a very small decoherence effect in DQD charge qubits. Since double-dot *spin* qubits are also susceptible to decoherence due to charge motion, in Sec. VII we use results from our circuit model of electromagnetic fluctuations to estimate decoherence rates for those system. Our conclusions are presented in Sec. VIII.

II. HAMILTONIAN OF THE DOUBLE-QUANTUM-DOT SYSTEM

The Hamiltonian of a DQD can be separated into a quantum part related to the occupation of energy levels on each dot and a classical part that quantifies the charging energy,

$$H = \sum_n \varepsilon_{1n} c_{1n}^\dagger c_{1n} + \sum_n \varepsilon_{2n} c_{2n}^\dagger c_{2n} + E(N_1, N_2), \qquad (1)$$

where $c_{in}^\dagger$ and c_{in} are creation and annihilation operators of the state with energy ε_{in} in the left ($i=1$) or right dot ($i=2$). The dot occupation numbers are defined as $N_i = \Sigma_n c_{in}^\dagger c_{in}$ while the total charging energy is given by[22]

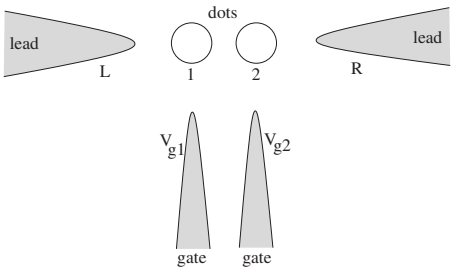

FIG. 1. Schematic representation of a double-quantum-dot setup.

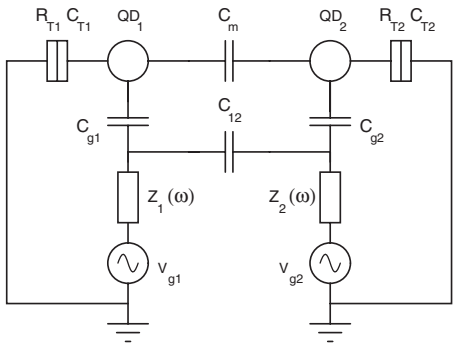

FIG. 2. Circuit representation of a double-quantum-dot system coupled to an electromagnetic environment through metallic gate electrodes. Source and drain electrodes are assumed grounded. The quantum dots are denoted by QD_1 and QD_2.

$$E(N_1,N_2) = \frac{E_{C1}}{2}N_1^2 + \frac{E_{C2}}{2}N_2^2 + N_1N_2E_{Cm} - \frac{1}{|e|}[C_{g1}V_{g1}(N_1E_{C1} + N_2E_{Cm})] - \frac{1}{|e|}[C_{g2}V_{g2}(N_1E_{Cm} + N_2E_{C2})] + \frac{1}{2e^2}[C_{g1}^2V_{g1}^2E_{C1} + C_{g2}^2V_{g2}^2E_{C2}] + \frac{1}{e^2}[C_{g1}V_{g1}C_{g2}V_{g2}E_{Cm}] \quad (2)$$

with the individual charging energies defined as

$$E_{C1} = \frac{e^2}{C_1}\left(1 - \frac{C_m^2}{C_1C_2}\right)^{-1}, \quad (3)$$

$$E_{C2} = \frac{e^2}{C_2}\left(1 - \frac{C_m^2}{C_1C_2}\right)^{-1}, \quad (4)$$

$$E_{Cm} = \frac{e^2}{C_m}\left(\frac{C_1C_2}{C_m^2} - 1\right)^{-1}. \quad (5)$$

The capacitances and voltages shown in Eqs. (2)–(5) are defined in Fig. 2. $C_{1,2}$ is the sum of all capacitances attached to dot 1 or 2: $C_{1,2}=C_{T1,2}+C_{g1,2}+C_m$.

For the purpose of our analysis, the Hamiltonian can be greatly simplified. Notice that the DQD qubit can be viewed as a double-well potential where an unpaired electron oscillates between both quantum dots by tunneling through the potential barrier. Spin degrees of freedom can be neglected. By adjusting the gate voltages, one can set the system near the degeneracy point $E(1,0)=E(0,1)$ in which case the logical states of the qubit correspond to the electron being on the left or right, $|L\rangle$ ($N_1=1$ and $N_2=0$) and $|R\rangle$ ($N_1=0$ and $N_2=1$), respectively. The typical single-particle level spacing within each quantum dot is assumed sufficiently large so that only one level on each dot needs to be considered at low enough temperatures. The barrier height Δ determines the tunneling rate between the dots and can be adjusted by a gate voltage while a bias ε between the two dots can also be applied through two independent plunger gate voltages. The dynamics in the DQD qubit is then governed by the reduced two-level Hamiltonian

$$H_S = \frac{\varepsilon}{2}(|L\rangle\langle L| - |R\rangle\langle R|) + \frac{\Delta}{2}(|L\rangle\langle R| + |R\rangle\langle L|) \quad (6)$$

with the constraint that $|L\rangle\langle L|+|R\rangle\langle R|=1$. The fields ϵ and Δ represent the interdot bias and the interdot capacitive coupling, respectively.

Electromagnetic noise is introduced into the DQD qubit system by means of gate-voltage fluctuations. These fluctuations may originate from the voltage sources and the thermal noise in the transmission lines, and introduce decoherence into the qubit system through interactions with the electrons in the quantum dots. While the former can be substantially reduced by careful filtering, the latter is less controlled. Here we will focus on the noise coming from the plunger gates. The effect of voltage fluctuations in the gate electrodes is captured by the qubit-environment interaction

$$H_{SB} = e\,\eta(\delta V_{g1} - \delta V_{g2})(|L\rangle\langle L| - |R\rangle\langle R|), \quad (7)$$

where η is the capacitive lever arm coefficient,

$$\eta = \frac{C_{g1}C_2 + C_{g2}C_1 - C_m(C_{g1} + C_{g2})}{4(C_1C_2 - C_m^2)}. \quad (8)$$

Depending on the particular qubit setup, other sources of electromagnetic noise may also exist, such as bias and current-voltage fluctuations. They can affect not only the qubit coherent dynamics but also the state measurement. For the sake of maintaining some generality in our study, we will only treat electromagnetic fluctuations which can be expressed as Eq. (7). In addition, we will model the voltage fluctuations through frequency-dependent impedances along the gate transmission lines.

III. HAMILTONIAN FOR THE ELECTROMAGNETIC ENVIRONMENT

The effective circuit of a double-quantum-dot setup is shown in Fig. 2. The effect of the electromagnetic environment is modeled by the frequency-dependent impedances $Z_{1,2}(\omega)$. In the experimental setups, the voltage lines typically run parallel to each other over several microns or more. In order to take into account any capacitive coupling between the lines, we introduced capacitance C_{12} into the circuit.

The impedances $Z_{1,2}(\omega)$ can be modeled by means of a transmission line with distributed elements, which stems from the fact that the source of noise in our circuit is spatially distributed along a finite length. Let us consider first each transmission line independently, as shown in Fig. 3, whose impedance $Z_i(\omega)$ can be represented by an infinite ladder network of identical inductors L_{ti} and capacitors C_{ti} (see Ref. 23),

$$Z_i(\omega) = \frac{1}{2}\left(i\omega L_{ti} + \sqrt{-\omega^2L_{ti}^2 + 4\frac{L_{ti}}{C_{ti}}}\right). \quad (9)$$

Typically, it would be necessary to estimate the values of the spatially distributed resistance, capacitance, and inductance

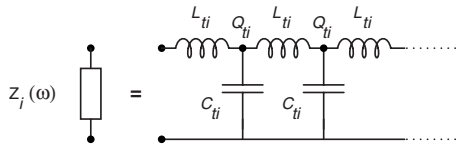

FIG. 3. Circuit representation of the electromagnetic environment as a transmission line.

in the circuit but the choice to model the impedance as a *LC* transmission line can be made because it is known that through a (not necessarily trivial) normal-mode transformation, any *RLC* or *RC* transmission line can be written as an infinite LC ladder network. The elements C_{ti} and L_{ti} of the transmission line can be determined from two real parameters of the real: the cutoff frequency ω_c and the low-frequency asymptotic limit to the characteristic impedance $Z(\omega=0)$. In an semi-infinite line, $\mathrm{Re}\{Z(\omega)\}=0$ when $\omega \geq \omega_c$. Hence,

$$\omega_c = \frac{2}{\sqrt{L_{ti}C_{ti}}}. \tag{10}$$

$Z_i(\omega=0)$, on the other hand, can be calculated by taking the low-frequency asymptotic limit of Eq. (9). It is straightforward to see that this limit yields

$$Z_i(\omega=0) = \sqrt{\frac{L_{ti}}{C_{ti}}} = R, \tag{11}$$

where R is an ohmic resistance.

To introduce noise, the transmission line is decomposed into normal modes. In quantized form, the charge at the lth node, $Q_{l,i}$, and the flux $\phi_{l,i}$ are conjugated variables obeying the commutation relation $[\phi_{l,i}, Q_{l',i'}] = ie\delta_{i,i'}\delta_{l,l'}$. Following the standard procedure, we define the Hamiltonian governing the flux and charge fluctuations along such transmission as

$$H_{T,i} = \frac{Q_{0,i}^2}{2C_{gi}} + \sum_{l=1}^{+\infty}\left[\frac{Q_{l,i}^2}{2C_{ti}} + \frac{\hbar^2}{e^2}\frac{(\phi_{l,i}-\phi_{l-1,i})^2}{2L_{ti}}\right]. \tag{12}$$

Notice that C_{gi} represents the capacitive coupling between the quantum dots and their respective gates while C_{ti} and L_{ti} represent the capacitive and inductive terms, respectively, at each rung in the transmission line.

Adding the capacitive coupling between the voltage transmission lines, we obtain the following environmental noise Hamiltonian:

$$H_B = H_{T,1} + H_{T,2} + \frac{Q_{0,1}Q_{0,2}}{C_{12}}. \tag{13}$$

The cross term complicates the task of finding the normal models of the environment and an alternative approach was adopted.

IV. DOUBLE-DOT JUNCTION

The double junction solution is based on the original solution for a single-dot junction treated in detail by Ingold and Nazarov.[24] The nontrivial aspect of our extension of the calculations in Ref. 24 is the inclusion of the gate capacitances (see Fig. 4).

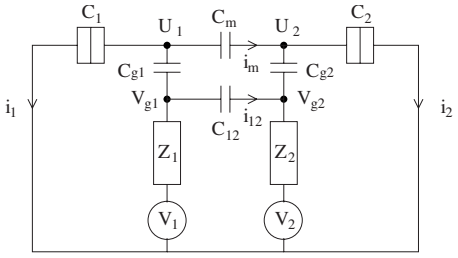

FIG. 4. Circuit of a double-dot junction system coupled to two voltage sources through noisy lines.

We start with the setup shown in Fig. 4. Following a straightforward application of Kirchhoff's laws, we find the relations

$$V_1 = (i_1 + i_{12} + i_m)Z_1 + V_{g1}, \tag{14}$$

$$V_2 = (i_1 - i_{12} - i_m)Z_2 + V_{g2} \tag{15}$$

with

$$V_{g1} - V_{g2} = i_{12}Z_{12} \tag{16}$$

and

$$U_1 - U_2 = i_m Z_m, \tag{17}$$

where $Z_{12}=(i\omega C_{12})^{-1}$ and $Z_m=(i\omega C_m)^{-1}$.

We begin by eliminating i_{12} and i_m in Eqs. (14) and (15) with the help of Eqs. (16) and (17), and proceed to write V_{g1} and V_{g2} in terms of U_1 and U_2. For this purpose, we notice that

$$V_{g1} = U_1 + (i_1 + i_m)Z_{g1},$$

$$V_{g2} = U_2 + (i_2 - i_m)Z_{g2},$$

$C_iU_i=Q_i$, and $i_1=\dot{Q}_1$, with $i=1,2$. Eliminating V_{g1}, V_{g2} and rewriting V_1, V_2 in terms of i_1, i_2, Q_1 and Q_2, we obtain, in matrix notation

$$\begin{pmatrix} V_1 \\ V_2 \end{pmatrix} = \mathcal{Z}\cdot\begin{pmatrix} \dot{Q}_1 \\ \dot{Q}_2 \end{pmatrix} + \tilde{\mathcal{C}}^{-1}\cdot\begin{pmatrix} Q_1 \\ Q_2 \end{pmatrix}, \tag{18}$$

where

$$\mathcal{Z} = \begin{pmatrix} \mathcal{Z}_{11} & \mathcal{Z}_{12} \\ \mathcal{Z}_{21} & \mathcal{Z}_{22} \end{pmatrix} \tag{19}$$

with

$$\mathcal{Z}_{11} = Z_1\left(1+\frac{C_m}{C_1}\right) + Z_1C_{12}\left[\frac{1}{C_1}\left(1+\frac{C_m}{C_{g1}}\right) + \frac{1}{C_{g1}} + \frac{C_m}{C_{g2}C_1}\right], \tag{20}$$

$$\mathcal{Z}_{12} = -Z_1\frac{C_m}{C_2} - Z_1C_{12}\left[\frac{C_m}{C_{g1}C_2} + \left(1+\frac{C_m}{C_{g2}}\right)\frac{1}{C_2} + \frac{1}{C_{g2}}\right], \tag{21}$$

$$\mathcal{Z}_{21} = -Z_2\frac{C_m}{C_1} - Z_2C_{12}\left[\frac{C_m}{C_{g2}C_1} + \left(1+\frac{C_m}{C_{g1}}\right)\frac{1}{C_1} + \frac{1}{C_{g1}}\right], \tag{22}$$

$$\mathcal{Z}_{22} = Z_2\left(1+\frac{C_m}{C_2}\right) + Z_2C_{12}\left[\frac{1}{C_2}\left(1+\frac{C_m}{C_{g2}}\right) + \frac{1}{C_{g2}} + \frac{C_m}{C_{g1}C_2}\right]. \tag{23}$$

The matrix $\tilde{C}$ is defined as

$$\tilde{C} = \frac{1}{\det(\tilde{C}^{-1})}\begin{pmatrix} \left[1+\frac{C_m}{C_{g2}}\right]\frac{1}{C_2} + \frac{1}{C_{g2}} & \frac{C_m}{C_{g1}C_2} \\ \frac{C_m}{C_{g2}C_1} & \left[1+\frac{C_m}{C_{g1}}\right]\frac{1}{C_1} + \frac{1}{C_{g1}} \end{pmatrix}, \tag{24}$$

where

$$\det(\tilde{C}^{-1}) = -\frac{C_m^2}{C_{g1}C_{g2}C_1C_2} + \left[\left(1+\frac{C_m}{C_{g1}}\right)\frac{1}{C_1} + \frac{1}{C_{g1}}\right]\left[\left(1+\frac{C_m}{C_{g2}}\right)\frac{1}{C_2} + \frac{1}{C_{g2}}\right]. \tag{25}$$

Notice that when we set $C_m=0$ and $C_{12}=0$ in Eq. (18), we decouple the two halves of the circuit and obtain two independent equations for each half of the circuit.

In analogy to the single-dot junction circuit, the Hamiltonian for the environment in this case can be written as

$$H_{\rm env} = H_{\rm charge} + \sum_{n=1}^{\infty}\frac{q_{n1}^2}{2C_{n1}} + \left(\frac{\hbar}{e}\right)^2\frac{(\tilde{\varphi}_{g1}-\varphi_{n1})^2}{2L_{n1}} + \frac{q_{n2}^2}{2C_{n2}} + \left(\frac{\hbar}{e}\right)^2\frac{(\tilde{\varphi}_{g2}-\varphi_{n2})^2}{2L_{n2}}. \tag{26}$$

We find that

$$\dot{q}_{ni}(t) = G_{ni}(t) + \frac{\hbar}{eL_{ni}}\int_0^t dt'\,\cos[\omega_{ni}(t-t')]\dot{\tilde{\varphi}}_{gi}(t'), \tag{27}$$

where $\omega_{ni}=1/\sqrt{L_{ni}C_{ni}}$ and

$$G_{ni}(t) = -\frac{\hbar}{eL_{ni}}\left[\frac{\sin(\omega_{ni}t)\dot{\varphi}_{ni}(0)}{\omega_{ni}} + \cos(\omega_{ni}t)\varphi_{ni}(0)\right]. \tag{28}$$

In addition, it is easy to show that the relation $\dot{\tilde{Q}}_i=-\Sigma_{n=1}^{\infty}\dot{q}_{ni}$ also hold. Thus, we can write

$$\dot{\tilde{Q}}_i(t) + \frac{\hbar}{e}\int_0^t dt'\,Y_i(t-t')\dot{\tilde{\varphi}}_{gi}(t') = I_{Ni}(t), \tag{29}$$

where the parameters $\{C_{ni},L_{ni}\}$ must be chosen such that

$$Y_i(t) = \sum_{n=1}^{\infty}\frac{\cos(\omega_{ni}t)}{L_{n1}} \to Y_i(\omega) = \frac{1}{Z_i(\omega)} \tag{30}$$

and

$$I_{Ni}(t) = -\sum_{n=1}^{\infty}G_{ni}(t). \tag{31}$$

Voltage correlation functions

We now turn the charge equation of motion, Eq. (29), into one for phase fluctuations, by using the following relationship:

$$\dot{\tilde{\varphi}}_g = \frac{e}{\hbar}(V_g - V) \tag{32}$$

and

$$V_g = \frac{Q}{\tilde{C}} = \frac{\tilde{Q}}{\tilde{C}} + V. \tag{33}$$

Substituting Eq. (33) into Eq. (32), we arrive at

$$\dot{\tilde{\varphi}}_g = \frac{e}{\hbar}\frac{\tilde{Q}}{\tilde{C}}, \tag{34}$$

which allows us to retrieve the phase fluctuation equation of motion,

$$\tilde{C}\cdot\ddot{\tilde{\varphi}}_g(t) + \int_0^t dt'\,\mathcal{Y}(t-t')\dot{\tilde{\varphi}}_g(t') = \frac{e}{\hbar}\mathcal{I}_N(t). \tag{35}$$

Since we are interested in the behavior of a double-dot junction, with each dot possessing its own charge and phase fluctuations, we will from now on represent these quantities in a vector notation, as seen in Eq. (35). By applying a Fourier transformation and substituting the random internal currents by external ones, we get

$$i\omega\mathcal{Z}_t^{-1}(\omega)\cdot\tilde{\tilde{\varphi}}_g(\omega) = \frac{e}{\hbar}\mathcal{I}_{\rm pert}(\omega), \tag{36}$$

where

$$\mathcal{Z}_t^{-1}(\omega) = \mathcal{Z}^{-1}(\omega) + i\omega\tilde{C}. \tag{37}$$

Now, substituting the external currents by appropriate generalized force matrix,

$$\mathcal{F}_g(\omega) = \frac{\hbar}{e}\mathcal{I}_{\rm pert}(\omega), \tag{38}$$

we obtain

$$\tilde{\tilde{\varphi}}_g(\omega) = \mathcal{X}_{\varphi_g}(\omega)\cdot\mathcal{F}_g(\omega), \tag{39}$$

where the dynamical susceptibility matrix is given by

$$\mathcal{X}_{\varphi_g}(\omega) = \left(\frac{e}{\hbar}\right)^2\frac{1}{i\omega}\mathcal{Z}_t(\omega), \tag{40}$$

whose imaginary part is given by

$$\mathcal{X}''_{\varphi_g}(\omega) = -\left(\frac{e}{\hbar}\right)^2 \frac{\mathrm{Re}\{\mathcal{Z}_t(\omega)\}}{\omega}. \tag{41}$$

Assuming that both transmission lines are at the same temperature, the generalized form of the fluctuation-dissipation theorem reads

$$\begin{aligned}
&\begin{pmatrix} \langle|\tilde{\varphi}_{g1}(\omega)|^2\rangle & \langle\tilde{\varphi}^*_{g1}(\omega)\tilde{\varphi}_{g2}(\omega)\rangle \\ \langle\tilde{\varphi}^*_{g2}(\omega)\tilde{\varphi}_{g1}(\omega)\rangle & \langle|\tilde{\varphi}_{g2}(\omega)|^2\rangle \end{pmatrix} \\
&= \int_{-\infty}^{\infty} dt e^{-i\omega t} \begin{pmatrix} \langle\tilde{\varphi}_{g1}(t)\tilde{\varphi}_{g1}(0)\rangle & \langle\tilde{\varphi}_{g1}(t)\tilde{\varphi}_{g2}(0)\rangle \\ \langle\tilde{\varphi}_{g2}(t)\tilde{\varphi}_{g1}(0)\rangle & \langle\tilde{\varphi}_{g2}(t)\tilde{\varphi}_{g2}(0)\rangle \end{pmatrix} \\
&= \frac{-2\hbar}{1-e^{-\beta\hbar\omega}} \mathcal{X}''_{\varphi_g}(\omega).
\end{aligned} \tag{42}$$

Hence,

$$\begin{aligned}
&\begin{pmatrix} \langle|\tilde{\varphi}_{g1}(\omega)|^2\rangle & \langle\tilde{\varphi}^*_{g1}(\omega)\tilde{\varphi}_{g2}(\omega)\rangle \\ \langle\tilde{\varphi}^*_{g2}(\omega)\tilde{\varphi}_{g1}(\omega)\rangle & \langle|\tilde{\varphi}_{g2}(\omega)|^2\rangle \end{pmatrix} \\
&= \left(\frac{e}{\hbar}\right)^2 \frac{2\hbar}{\omega} \frac{1}{1-e^{-\beta\hbar\omega}} \mathrm{Re}\{\mathcal{Z}_t(\omega)\}.
\end{aligned} \tag{43}$$

We now turn to the fluctuations of the voltage at the dots. Since

$$\begin{pmatrix} \delta U_1 \\ \delta U_2 \end{pmatrix} = \mathcal{C}^{-1} \cdot \begin{pmatrix} \delta\tilde{Q}_1 \\ \delta\tilde{Q}_2 \end{pmatrix} = \frac{\hbar}{e} \mathcal{C}^{-1} \cdot \tilde{\mathcal{C}} \cdot \begin{pmatrix} \dot{\tilde{\varphi}}_{g1} \\ \dot{\tilde{\varphi}}_{g2} \end{pmatrix}, \tag{44}$$

where

$$\mathcal{C} = \begin{pmatrix} C_1 & 0 \\ 0 & C_2 \end{pmatrix}, \tag{45}$$

we find the matrix equation

$$\mathcal{U} = \frac{2\hbar\omega}{1-e^{-\beta\hbar\omega}} \mathcal{M}, \tag{46}$$

where

$$\mathcal{M} = \mathcal{C}^{-1} \cdot \tilde{\mathcal{C}} \cdot \mathrm{Re}\{\mathcal{Z}_t(\omega)\} \cdot \tilde{\mathcal{C}}^\dagger \cdot (\mathcal{C}^{-1})^\dagger \tag{47}$$

and

$$\mathcal{U} = \begin{pmatrix} \langle|\delta U_1(\omega)|^2\rangle & \langle\delta U_1^*(\omega)\delta U_2(\omega)\rangle \\ \langle\delta U_2^*(\omega)\delta U_1(\omega)\rangle & \langle|\delta U_2(\omega)|^2\rangle \end{pmatrix}. \tag{48}$$

V. ESTIMATE OF CIRCUIT PARAMETERS

We now proceed to make realistic estimates of the effective circuit parameters. The double-dot system is maintained at very low temperatures, in the tens of millikelvin.[25] Typically, $k_B T \ll \Delta E, E_{C1}, E_{C2}$, where ΔE is the mean level spacing in the dots. The wires leading to the double quantum dot are thermally anchored to a fridge at several temperature stages (4 K, 1 K, 100 mK, and 10 mK). The transmission line resistance R_L is estimated to be 50 Ω for low temperatures (at or below 4 K) inside the dilution refrigerator, or 250 Ω in the copper leads residing at room temperature.[26]

The resistance of the two-dimensional electron gas (2DEG) can be calculated using Drude's theory.[27] The typical electron density in a high-mobility GaAs 2DEG is approximately $n=10^{11}$ cm^{-2}, which leads to an average Fermi velocity of about $v_F=10^5$ m/s. At subkelvin temperatures, mean-free paths in the 2DEG range from a few to up to 1 μm.[28] Choosing $l=10$ μm, we arrive at a relaxation time $\tau=l/v_F \approx 100$ ps, leading to an estimate of the low-temperature conductivity of

$$\sigma = \frac{ne^2\tau}{m^\star} \simeq 4.2 \times 10^{-2} \text{ S} \tag{49}$$

with $m^\star = 0.067 m_e = 0.61 \times 10^{-31}$ kg being the electron effective mass in GaAs. To calculate the resistance, we considered a length $l=10$ μm and a width $w=2.5$ μm, yielding a sheet resistance for the 2DEG underneath the gate electrodes

$$R_s = \rho \frac{l}{w} \simeq 95 \ \Omega/\square, \tag{50}$$

where $\rho = 1/\sigma$ is the resistivity of the 2DEG. This resistance is responsible for a dissipative drag effect[29] that, for the sake of simplicity, will not be considered in our model.

There is still one resistance left to be determined, which is the resistance of the metallic electrodes. This resistance can be determined by

$$R = \rho \frac{l}{bc}, \tag{51}$$

where ρ is the resistivity of the electrodes, approximately 0.022×10^{-8} Ωm for a Au electrode at low temperature (<4 K). If we consider the electrodes to have a 10 μm length and a 30 nm $\times$ 60 nm cross section, we can estimate the electrode resistance to be around 1 Ω, a small value that will also not be considered in our model.

The capacitance C between the transmission line and the 2DEG was estimated by solving the electromagnetic problem of a cylindrical conducting wire of radius $r=20$ nm placed at a distance of $d=100$ nm from an infinite grounded conducting plate. Using the method of images, we can estimate the total electric potential of this system by integrating the electric field along the line connecting the centers of the real and the image wires. This results in a capacitance per unit length of 25 aF/μm, and a total capacitance of 250 aF for a wire of 10 μm in length.

Any inductive couplings along our voltage lines can be estimated as follows. For a metal electrode with rectangular cross section, the self-inductance in H/m is approximated as[30]

$$L_{\mathrm{rod}} \sim 2l \left[\ln\left(\frac{2l}{b+c}\right) - \ln \epsilon + \frac{1}{2} \right] \times 10^{-7}, \tag{52}$$

where ϵ is the aspect ratio of the electrode. For an electrode with an aspect ratio of 2, this equation yields $L \approx 1$ pH/μm. Thus, a 10 μm long electrode gives us an inductance of 10 pH. The parameters $C=250$ aF and $L=10$ pH, though useful as rough estimates to characterize circuits, will not be used in our model since they are very specific to the given circuit. In fact, in order to estimate these

TABLE I. Estimates for the transmission line parameters.

Transmission line parameters	
Length l	10 μm
Transmission line capacitance C_t	10 pF
Transmission line inductance L_t	10 pH
Cutoff frequency ω_c	200×10^9 rad/s
$Z(\omega=0)=R$	1 Ω

circuit elements more precisely, more physical parameters of the circuit in question would be necessary. To determine the transmission line parameters in our model, we will make use of Eqs. (10) and (11) from Sec. III to give us a more general approach where we can model any transmission line given these two operating parameters. To give us a large enough window to operate our qubits, we set our cutoff frequency to $\omega_c=200\times10^9$ rad/s. Table I summarizes the transmission line parameters that fully describe $Z_i(\omega)$.

The gate capacitance $C_{gi}(i=1,2)$ for each quantum dot is given by

$$C_{gi}=\frac{|e|}{\Delta V_{gi}}. \tag{53}$$

If we consider $\Delta V_{gi}\approx4.5$ mV,[22,25] we find $C_{gi}\approx40$ aF.

Finally, we now estimate the tunneling parameters between the quantum dots and the 2DEG. These are given by a tunneling junction with an impedance $Z_T=R_T+jX_{C_T}$. We can obtain a lower bound for the tunneling resistance R_T by estimating the inverse of the Coulomb blockade peak conductance. In the regime $\Gamma\ll k_BT$, $G_{\max}$ is given by[31]

$$G_{\max}=\frac{e^2}{4k_BT}\frac{\Gamma^l\Gamma^r}{\Gamma^l+\Gamma^r}, \tag{54}$$

where tunneling rates of an electron through the potential barrier into (or out of) each dot are assumed equal for the sake of simplicity ($\Gamma^l=\Gamma^r$) For an electron temperature in the dot $T\approx150$ mK and a peak conductance height of $2\times10^{-3}e^2/h$,[7] we find the tunneling resistance to be larger than or on the order of 10 MΩ. We can estimate the tunneling capacitance indirectly. We know the expression for the total capacitance of a flat disk to be

$$C_i=8\epsilon_r\epsilon_0R. \tag{55}$$

Assuming $R\approx80$ nm as the radius of the quantum dot and $\epsilon_r\approx11$ for GaAs at high frequencies, yielding a total capacitance $C_i\approx60$ aF for each quantum dot.

From the total capacitance we can estimate the interdot capacitance between dots 1 and 2 since

$$C_m=\frac{\Delta V_{gi}^m}{\Delta V_{gi}}C_j, \tag{56}$$

where $i\neq j$. For $\Delta V_{gi}^m\approx0.4$ mV,[22,25] we find $C_m\approx5$ aF.

The total capacitance for each quantum dot, as seen previously, is the sum of all capacitances attached to the dot. As such, by knowing $C_m=5$ aF and $C_{Ti}=40$ aF, we find $C_{gi}\approx15$ aF.

TABLE II. Estimates for the DQD circuit parameters. $i=1,2$ corresponding to each quantum dot.

Circuit parameters	
Transmission line capacitance C_{ti}	1 pF/μm
Transmission line inductance L_{ti}	1 pH/μm
Interdot capacitance C_m	5 aF
Tunneling capacitance C_{Ti}	40 aF
Tunneling resistance R_{Ti}	$\gtrapprox10$ MΩ
Gate capacitance C_{gi}	15 aF
Total quantum dot capacitance C_i	60 aF
Capacitive coupling between transmission lines C_{12}	$\simeq20$ aF
Electrode resistance R_i	1 Ω

Using these estimates for the circuit elements, we are able to determine the distributed parameters of our noisy transmission lines. According to Eq. (11), if we assume a cutoff frequency of $\omega_c\sim10^{11}$ Hz, we find $L_{ti}\sim1$ pH/μm and $C_{ti}\sim1$ pF/μm.

In principle, one can also consider the ground (2DEG) to be a source of noise, and as such it can also be modeled by means of a frequency-dependent impedance. This would require however an appropriate estimate of the inductance along the 2DEG. We did not carry out such an estimate. However, we attempt to take into account the coupling between the quantum dot leads. This coupling is given by the lumped capacitance C_{12}, as shown in Fig. 2. This capacitance was estimated to be approximately 20 aF by means of numerical multipole expansion calculations performed by a field solver software.[32] We summarize in Table II the relevant circuit parameters necessary to fully characterize the DQD setup.

VI. BOUNDS ON DECOHERENCE RATES AND Q FACTORS

Through the fluctuation-dissipation theorem, we can relate the impedance $Z_{1,2}(\omega)$ to a source of electromagnetic gate fluctuations $\delta V_{g1,2}$. These gate fluctuations $\delta V_{gi}=Q_{0,i}/C_{gi}(i=1,2)$ can be determined through the diagonalization of the Hamiltonian in Eq. (12). We consider in this paper the case of Johnson-Nyquist noise.[33,34] Following the standard procedure, we relate the energy relaxation rate to the power spectrum of voltage fluctuations,

$$\gamma_1=\frac{\sin^2\eta}{4\hbar^2}\left[\frac{S_{\delta U}(\Delta/\hbar)+S_{\delta U}(-\Delta/\hbar)}{2}\right], \tag{57}$$

where

$$S_{\delta U}(\omega)=\frac{e^2}{2}\langle|[\delta U_1(\omega)-\delta U_2(\omega)]|^2\rangle \tag{58}$$

and $\tan\eta=\Delta/\epsilon$, see Eq. (46). Using Eq. (6), we obtain

$$\gamma_1 = \frac{\sin^2 \eta\Delta}{\hbar R_K} \coth\left(\frac{\Delta}{2k_B T}\right)\tilde{\mathcal{M}}, \tag{59}$$

where

$$\tilde{\mathcal{M}} = \mathcal{M}_{11} + \mathcal{M}_{22} - \mathcal{M}_{12} - \mathcal{M}_{21} \tag{60}$$

and R_K is the resistance quantum ($=h/e^2 \simeq 25.8$ kΩ). From this expression we can calculate the energy relaxation and dephasing times,

$$T_1 = 1/\gamma_1 = \frac{\hbar R_K}{\sin^2 \eta\Delta} \frac{\tanh(\Delta/2k_B T)}{\tilde{\mathcal{M}}} \tag{61}$$

and

$$T_2 = \left[\frac{1}{2T_1} + \frac{\cos^2 \eta}{4\hbar^2} S(\Delta/\hbar)\right]^{-1}. \tag{62}$$

Hereafter, we will assume zero bias ($\epsilon=0$) in which case $\eta = \pi/2$ and $T_2=2T_1$. The quality factor of the quantum oscillations is then given by

$$Q = \omega_{\rm osc} T_2 = \frac{\omega_{\rm osc}}{\pi\gamma_1}, \tag{63}$$

where $\omega_{\rm osc}$ is the frequency of quantum oscillations observed in the DQD system, as defined by[33]

$$\omega_{\rm osc} = \sqrt{2\frac{\Delta}{\hbar}\left(2\frac{\Delta}{\hbar} + \frac{\gamma_2}{2}\right) - \frac{\gamma_1^2}{4}} \tag{64}$$

with Δ being the potential barrier height between quantum dots, as shown in Eq. (6), and γ_2 being defined as

$$\gamma_2 = -\int_0^\infty \frac{dy}{y^2-1} \nu(2\Delta y) \coth\left(\frac{\Delta y}{k_B T}\right), \tag{65}$$

where ν is the bath spectral function, defined as

$$\nu(\omega) = \frac{2}{\pi}\frac{\omega}{R_K}\{\langle|\delta U_1(\omega)|^2\rangle + \langle|\delta U_2(\omega)|^2\rangle - \langle\delta U_1^*(\omega)\delta U_2(\omega)\rangle - \langle\delta U_2^*(\omega)\delta U_1(\omega)\rangle\}. \tag{66}$$

The operating frequency $\omega=2\Delta/\hbar$ is fed to the circuit by the voltage generators and carried through the gates. The other terms in Eq. (64), as it turns out, are small enough corrections to the operating frequency so that they may be ignored. Thus, from now on we will assume $\omega_{\rm osc}=\omega$. We will now analyze in detail two different scenarios: one where the transmission lines are decoupled while the other includes the capacitive coupling C_{12} between transmission lines, as seen in Fig. 2.

A. Case (i): Decoupled transmission lines

It is useful to look at the case where there is no coupling between the electrodes. The decoherence introduced by the electromagnetic voltage fluctuations can still be analyzed using Eqs. (59)–(63) but some simplifications to the impedance matrix are now possible. This case corresponds to having $C_{12}=0$, so the matrix $\mathcal{Z}$ from Eq. (19) is reduced to

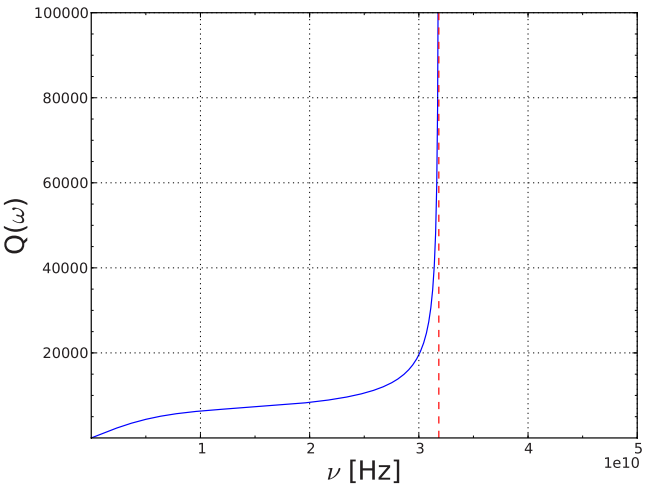

FIG. 5. (Color online) Qubit quality factor as a function of frequency for two decoupled semi-infinite transmission lines, with temperature $T=150$ mK and the circuit parameters presented in Table II.

$$\mathcal{Z} = \begin{pmatrix} Z_1\left(1+\frac{C_m}{C_1}\right) & -Z_1\frac{C_m}{C_2} \\ -Z_2\frac{C_m}{C_1} & Z_2\left(1+\frac{C_m}{C_2}\right) \end{pmatrix}. \tag{67}$$

In this case we observe the highest possible quality factors for our double-quantum-dot setup, as seen in Figs. 5 and 6.

If we look back at Eq. (63) and take its asymptotic limit for low frequencies, Eq. (67) is then reduced to

$$\mathcal{Z} = \begin{pmatrix} R_1\left(1+\frac{C_m}{C_1}\right) & -R_1\frac{C_m}{C_2} \\ -R_2\frac{C_m}{C_1} & R_2\left(1+\frac{C_m}{C_2}\right) \end{pmatrix}, \tag{68}$$

where $R_i=\mathcal{Z}(\omega=0)=\sqrt{L_{ti}/C_{ti}}$, as reported earlier, and with the assumption that $C_1=C_2$, $C_{g1}=C_{g2}$, and $R_1=R_2$. This,

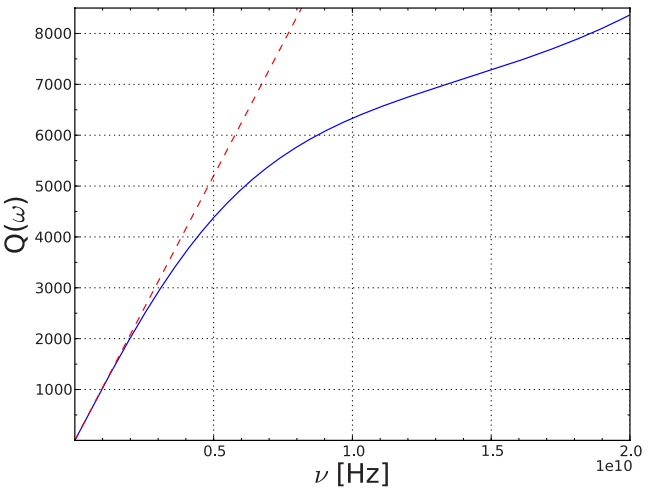

FIG. 6. (Color online) Qubit quality factor as a function of frequency for $\nu<20$ GHz and two decoupled semi-infinite transmission lines with the same parameter values as in Fig. 5.

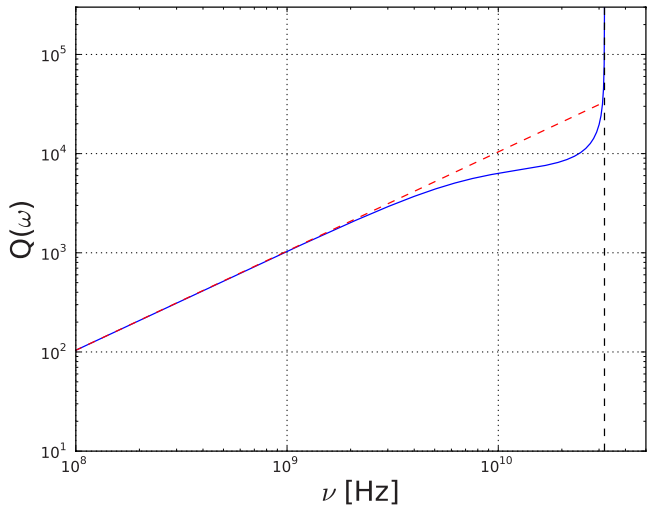

FIG. 7. (Color online) Quality factor as a function of frequency for two decoupled transmission lines represented in a logarithmic scale with the same parameter values as in Fig. 5.

combined with the fact that $\mathrm{Re}\{\mathcal{Z}_t(\omega)\}\to\mathrm{Re}\{\mathcal{Z}(\omega)\}$ for $\omega\to 0$, yields

$$\lim_{\omega\to 0} Q(\omega) = (8.9\times 10^{-7}\ [\mathrm{s}])\nu, \tag{69}$$

where we notice a linear dependence of Q with respect to ν, as can also be evidenced in the log-log graph shown in Fig. 7. While R_i is an important modeling parameter for the transmission lines, it is also clear that C_{ti} and L_{ti} ultimately influence how quickly this linear regime establishes itself once we move to lower frequencies.

Turning our attention now to higher frequencies, we notice an important characteristic of the transmission lines. The real part of the transmission line impedance $\mathrm{Re}\{\mathcal{Z}(\omega)\}$ has a cutoff frequency given by $\nu_c=\omega_c/2\pi$. In Fig. 8, it can be seen that as $\omega\to\omega_c$, $\mathrm{Re}\{\mathcal{Z}(\omega)\}\to 0$, making $\mathrm{Re}\{\mathcal{Z}_t(\omega)\}\to 0$ as well, causing the quality factor Q to diverge at $\omega=\omega_c$.

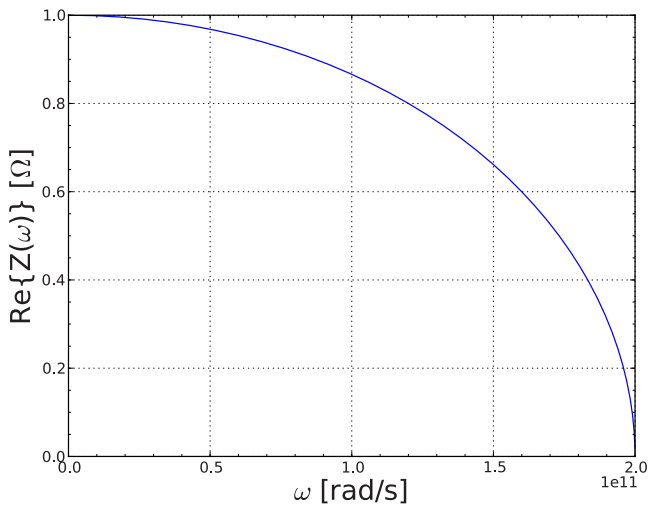

FIG. 8. (Color online) Real part of the impedance $\mathcal{Z}(\omega)$ as a function of the frequency ω. Transmission line parameters are defined in Table II.

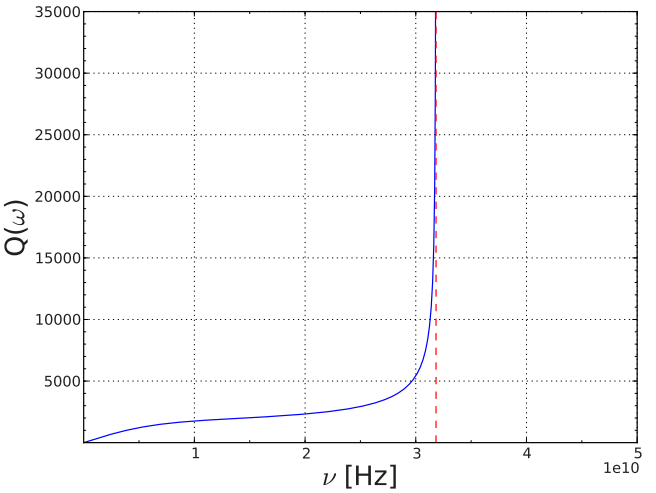

FIG. 9. (Color online) Qubit quality factor as a function of frequency, with temperature $T=150$ mK. The circuit parameters utilized are presented in Table II.

B. Case (ii): Capacitively coupled transmission lines

Inserting now the intercapacitive coupling C_{12} estimated in Sec. V, we obtain the quality factor Q as a function of frequency ν shown in Figs. 9–11. In Fig. 9, we can clearly observe the quality factor diverge at the frequency $\nu_c \simeq 320$ GHz, corresponding to the cutoff frequency. From now on we shall restrict our discussion to operating frequencies under 20 GHz (Fig. 11), which are more realistic for practical implementations of qubit operations.

It is interesting to observe the influence of temperature on the decoherence introduced into the system by voltage fluctuations. We show below, in Figs. 12 and 13, a family of Q factor curves as a function of operating frequency ν for temperatures ranging from 50 mK all the way to room tempera-

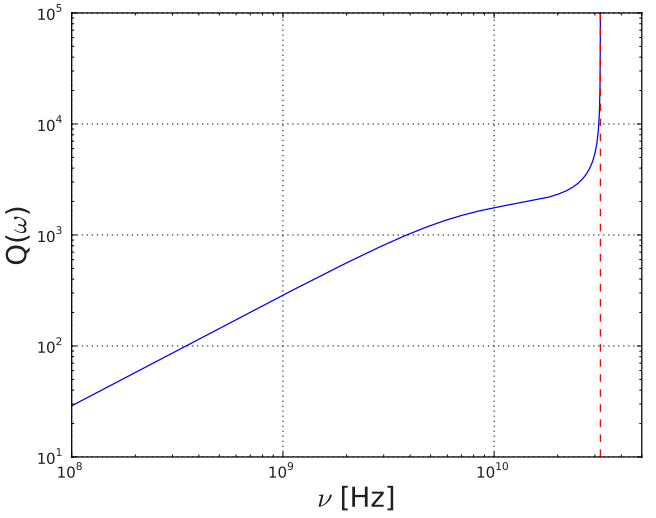

FIG. 10. (Color online) Qubit quality factor as a function of frequency represented in a logarithmic scale. The circuit parameters utilized are the same as in Fig. 9.

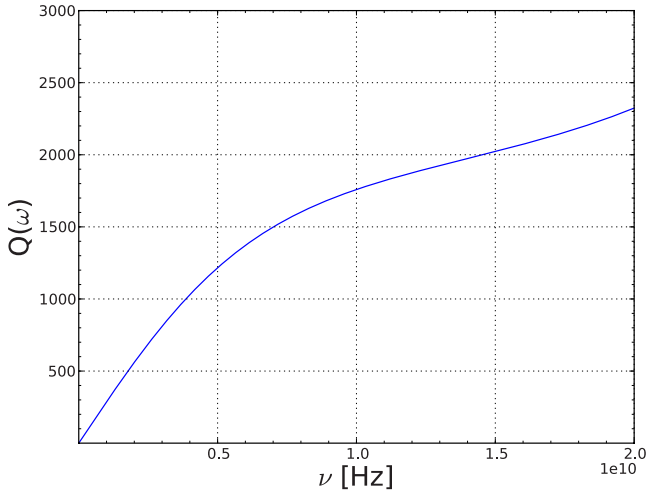

FIG. 11. (Color online) Quality factor as a function of frequency for $\nu<20$ GHz and two decoupled semi-infinite transmission lines with the same parameter values as in Fig. 9.

ture. As temperature increases, more environmental modes are available for the system to couple with, effectively increasing dissipative effects.

We can also observe the influence of the intercapacitive coupling C_{12} on the quality factor, as seen in Figs. 14 and 15. For weaker coupling, i.e., smaller C_{12}, the quality factors are higher, as C_{12} approaches the limiting case of decoupled lines. Note that $Q(\omega)$ will still not reach the same levels of the decoupled case due to the presence of the capacitance C_m.

In Tables III and IV we present the results of calculations for the decoherence time T_2 and the Q factor for several different values of temperature T and intercapacitive coupling C_{12}. It is easy to understand why higher temperatures degrade decoherence times in qubit operations. We can consider two extreme cases, namely, one where the electrical leads are inside a dilution refrigerator and another where they are at room temperature. We will also consider an operating frequency $\nu=\omega/2\pi$ of 10 GHz. First, let us assume that leads connected to the gate electrode are inside the dilution refrigerator. In this case, a temperature $T=150$ mK results in a relaxation time $T_1=88$ ns and a decoherence time of $T_2=176$ ns. This scenario yields a quality factor of $Q\approx1760$. If we consider now the case where the leads are at room temperature, we estimate the relaxation time and the dephasing time to be approximately 76 ps and 152 ps, respectively, resulting in a quality factor of $Q\simeq1.5$, more than 1000 times lower. A much more interesting analysis stems from varying the intercapacitive coupling between the transmission lines. For higher values of C_{12}, it would be intuitive to expect both transmission lines to be more strongly coupled, meaning that decoherence in the system would be weaker since voltage fluctuations in the two lines would be

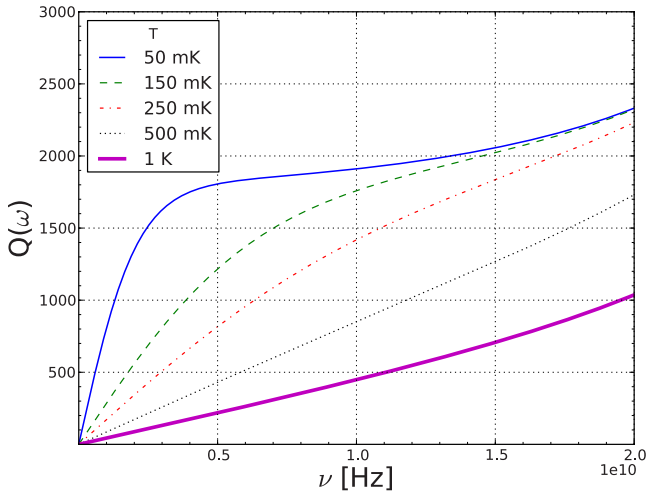

FIG. 12. (Color online) Qubit quality factor as a function of operating frequency for temperatures $T=50$, 150, 250, 500 mK, and 1 K. The circuit parameters utilized are presented in Table II.

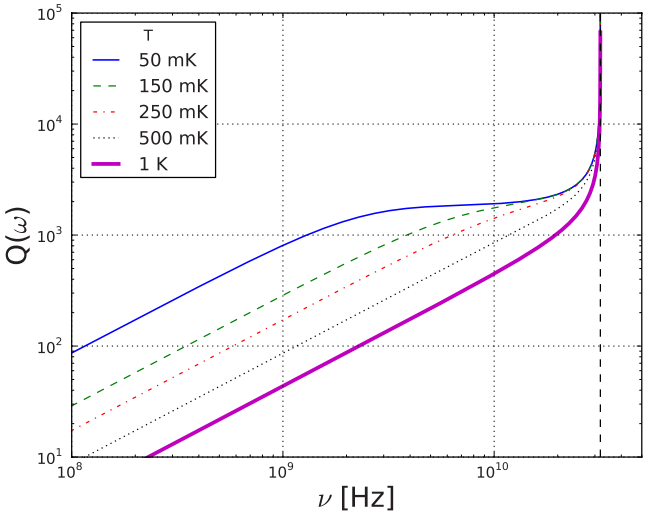

FIG. 13. (Color online) Logarithmic representation of the qubit quality factor as a function of operating frequency for temperatures $T=50$, 150, 250, 500 mK, and 1 K. The circuit parameters utilized are presented in Table II.

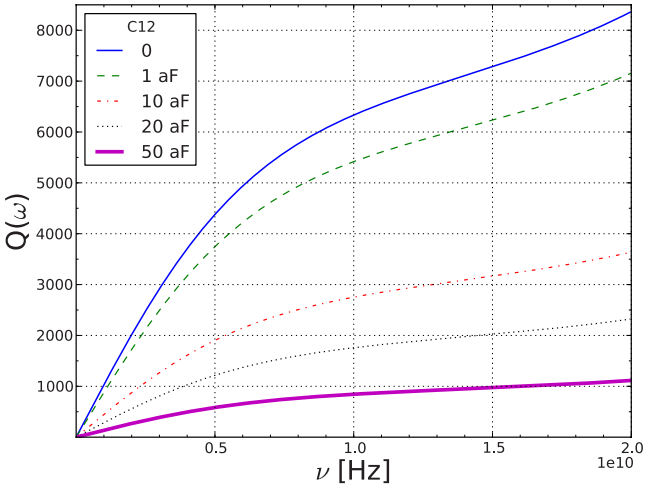

FIG. 14. (Color online) Quality factor as a function of operating frequency for temperature $T=150$ mK and intercapacitive couplings $C_{12}=0$, 1.3, 10, 20, and 50 aF. The circuit parameters utilized are presented in Table II.

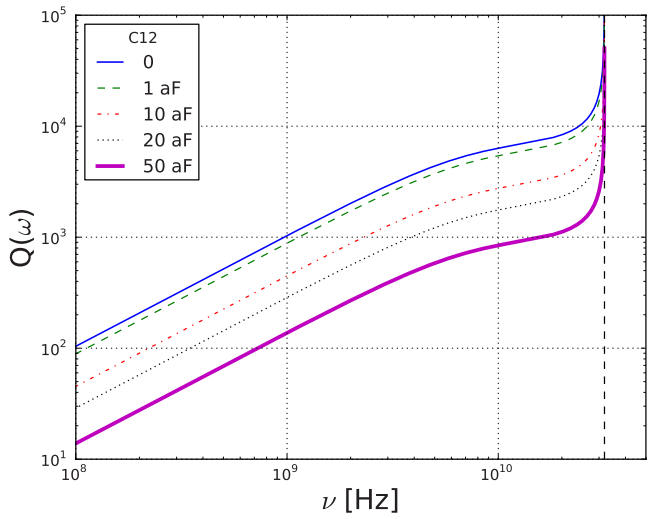

FIG. 15. (Color online) Logarithmic representation of the qubit factor as a function of operating frequency for temperature $T=150$ mK and intercapacitive couplings $C_{12}=0$, 1.3, 10, 20, and 50 aF. The circuit parameters utilized are the same as in Fig. 14.

correlated. As it turns out, however, the stronger coupling between transmission lines results in larger off-diagonal terms in the matrix of voltage correlations defined in Eq. (46). If we look at Eq. (63) once more, it is easy to see that larger off-diagonal terms subtracted from the main diagonal correlation terms results in smaller Q factors, as evidenced by the behavior of the family of Q factor curves in Fig. 14 for different values of intercapacitive coupling and the calculated values presented in Table IV.

VII. ELECTROMAGNETIC FLUCTUATIONS IN DOUBLE-DOT SPIN QUBITS

Decoherence due to the coupling between orbital (charge) and environmental degrees of freedom also occurs in certain spin-based quantum-dot qubits. For instance, in the double-dot system introduced by the Harvard group,[3] the computational basis is formed by the singlet and the $S_z=0$ triplet states of a DQD system possessing an overall excess of two electrons. Single qubit operations are performed by modulating the gate-voltage difference between the two dots, as well as through the coupling to an inhomogenous Overhauser field. For instance, calling the singlet states "up" and triplet state "down" pseudospin states, we can write the following pseudospin Hamiltonian

$$H_S = \left[\frac{\partial J}{\partial \varepsilon}(\varepsilon)\right] e\eta(V_1 - V_2), \sigma_z + H_{HF}, \tag{70}$$

where H_{HF} describes the coupling to the Overhauser field and $J(\varepsilon)$ is the effective exchange coupling. The latter can be calculated in second-order perturbation theory,

$$J(\varepsilon) = 4t^2\left[\frac{1}{(U-\varepsilon)} + \frac{1}{(U+\varepsilon)}\right] \tag{71}$$

with $t=\Delta/2$ denoting the interdot tunneling matrix element and $U=E_{C1}=E_{C2}$ representing the dot charging energy (for the sake of simplicity, we assume equal charging energy for both dots). The values $\varepsilon=\pm U$ mark the transitions from $(N_1=1,N_2=1)$ to $(N_1=2,N_2=0)$ or $(N_1=0,N_2=2)$ states and the breakdown of the perturbative expansion.

The first term in Eq. (70) is quite similar to first term in Eq. (6). Gate-voltage fluctuations will couple to this spin qubit similarly to the case of the DQD charge qubit.[35] Therefore, for small biases ($|\varepsilon| \ll U$), we can study decoherence induced by electromagnetic fluctuations in the spin qubit employing the same analysis developed in the previous sections for the charge qubit. We note that several studies of decoherence due to other mechanisms also present in these qubits have been done.[11,36,37]

The decoherence rates will depend strongly on the qubit operation point, given that the prefactor $|\partial J/\partial\varepsilon|$ appearing in Eq. (70) varies rapidly with ε. Qubit operations around this point require pulsing the exchange coupling $J(\varepsilon)$ for a time interval τ_E, during which the qubit may be vulnerable to dephasing due to electromagnetic fluctuations. An estimate of the corresponding decoherence time can be obtained by using the curve $J(\varepsilon)$ plotted in Fig. 3d of Ref. 3. Near $\varepsilon=-1$ mV, one finds $|\partial J/\partial\varepsilon| \approx 10^{-3}$. Since decoherence rates are proportional to the square of the bath-qubit coupling,

TABLE III. Estimates for the dephasing times T_2 for different values of temperature T and interline capacitive coupling C_{12}.

	Dephasing time T_2 (ns)				
			C_{12} (aF)		
T (K)	0	~1	10	20	50
50×10^{-3}	688	588	300	191	92
150×10^{-3}	633	542	275	176	84
250×10^{-3}	511	437	222	142	68
500×10^{-3}	306	262	133	85	41
1	161	138	70	45	22
300	0.55	0.47	0.24	0.15	0.07

TABLE IV. Estimates of Q factors for different values of temperature T and intercapacitive coupling C_{12}.

	Q factor				
0	~1	10	20	50	
50×10^{-3}	6878	5884	2990	1910	917
150×10^{-3}	6333	5418	2753	1760	844
250×10^{-3}	5108	4369	2220	1418	681
500×10^{-3}	3059	2617	1329	850	408
1	1614	1380	702	448	215
300	5.5	4.7	2.4	1.5	0.7

namely, $|\partial J/\partial\varepsilon|^2$ in this case, we conclude that the decoherence times due to electromagnetic fluctuations are 10^6 larger than those found for the DQD charge qubits, hence ranging from tens to hundreds of millisecond. In practice, these times are much larger than τ_E, which is typically a few hundreds of picosecond. We can conclude that gate-voltage fluctuations are also not a significant source of decoherence for spin qubits.

VIII. CONCLUSIONS

In this paper, we have modeled noise introduced by gate-voltage fluctuations in double-quantum-dot systems. We attempted to model the circuits leading to the DQD in a way that put us as close to real experimental values as possible while still being able to estimate all the relevant parameters and calculate decoherence rates and quality factors.

We chose to place our noise sources in our gates because we believe they give the largest contribution to decoherence during qubit operations. For additional considerations, noise sources could also be placed, for example, in the drain and source electrodes.

We have estimated the effect of fluctuations in the electrodes feeding the quantum dots and shown the influence that parameters such as temperature and intercapacitive coupling between electrodes have on decoherence in qubit operation. We have also shown that, similarly to decoherence by phonon coupling, temperature degrades coherence in the state superpositions, reinforcing the need for efficient refrigeration of the leads. This effect can be explained analogously to the radiation of a black body, which increases with temperature.

Contrary to what was initially expected, it was found that a stronger intercapacitive coupling between electrodes actually introduces stronger decoherence in the qubit system. Thus, in order to mitigate this effect, it is important to keep the leads gating each quantum dot in the system as isolated as possible from each other.

There are a few possible refinements to the model presented here. One such improvement includes adding the electrical resistance in the leads, which in practice requires the use of a lossy transmission line model for the effective circuit. It may also be important to take into account the drag effect on the leads due to the proximity to the 2DEG. This effect will change the effective circuit parameters, thus influencing the calculation of relaxation and dephasing times.

We have found that electromagnetic fluctuations in DQD systems do not introduce a dominating decoherence effect. The quality factors calculated for our system at room temperature (~210) are still well above the Q factors found in systems under the effect of phonon coupling (~50).[15–17,38] If we compare these results with the experimental results (~3–9) for Q factors, the discrepancy is even larger.[6–8]

The disagreement between theoretical estimates and measured decoherence times in charge-based DQD system leads us to believe that there must be another possible noise source that accounts for the short decoherence times observed in these systems. For instance, it has been recently argued that electron-electron interactions can enhance the effect of fluctuating background charges on the charge qubits.[39,40]

In order to identify the leading decoherence mechanism in charge-based qubits, it would be very helpful if the dependence of the Q factor on the qubit operating frequency ν were measured. For instance, for bosonic environments, this would yield the spectral function. With this information in hand, one could perhaps trace back the physical process underlying the decoherence mechanism. A candidate for such source is the presence of fluctuating background charges trapped in the insulating substrate or at the GaAS/GaAlAs interface.

ACKNOWLEDGMENTS

We are grateful to A. Chang, R. Hanson, and J. Kycia for providing us with information related to their experimental setups, as well as W. Coish, A. Fowler, E. Novais, and J. M. Taylor for useful discussions. This work was supported in part by the NSF under Grant No. CCF 0523603 and by the Office of Naval Research. D.C.B.V. and E.R.M. acknowledge partial support from the Interdisciplinary Information Science and Technology Laboratory (I^2Lab) at UCF. F.K.W. acknowledges support by NSERC through the Discovery Grants program and through QuantumWorks.

[1] D. Loss and D. P. DiVincenzo, Phys. Rev. A **57**, 120 (1998).
[2] R. H. Blick and H. Lorenz, in *Proceedings of the IEEE International Symposium on Circuits and Systems*, edited by J. Calder (IEEE, Piscataway, NJ, 2000), Vol. II, p. 245.
[3] J. R. Petta, A. C. Johnson, J. M. Taylor, E. A. Laird, A. Yacoby, M. D. Lukin, C. M. Marcus, M. P. Hanson, and A. C. Gossard, Science **309**, 2180 (2005).
[4] F. H. L. Koppens, C. Buizert, K. J. Tielrooij, I. T. Vink, K. C. Nowack, T. Meunier, L. P. Kouwenhoven, and L. M. K. Vandersypen, Nature (London) **442**, 766 (2006).
[5] T. Tanamoto, Physica B **272**, 45 (1999); Phys. Rev. A **61**, 022305 (2000).
[6] T. Hayashi, T. Fujisawa, H. D. Cheong, Y. H. Jeong, and Y. Hirayama, Phys. Rev. Lett. **91**, 226804 (2003); T. Fujisawa, T. Hayashi, H. D. Cheong, Y. H. Jeong, and Y. Hirayama, Physica E **21**, 1046 (2004).
[7] J. R. Petta, A. C. Johnson, C. M. Marcus, M. P. Hanson, and A. C. Gossard, Phys. Rev. Lett. **93**, 186802 (2004).
[8] J. Gorman, D. G. Hasko, and D. A. Williams, Phys. Rev. Lett. **95**, 090502 (2005).
[9] L. C. L. Hollenberg, A. S. Dzurak, C. Wellard, A. R. Hamilton, D. J. Reilly, G. J. Milburn, and R. G. Clark, Phys. Rev. B **69**, 113301 (2004).
[10] A. C. Johnson, J. R. Petta, J. M. Taylor, A. Yacoby, M. D. Lukin, C. M. Marcus, M. P. Hanson, and A. C. Gossard, Nature (London) **435**, 925 (2005).
[11] J. M. Taylor, J. R. Petta, A. C. Johnson, A. Yacoby, C. M. Marcus, and M. D. Lukin, Phys. Rev. B **76**, 035315 (2007).
[12] L. Fedichkin, M. Yanchenko, and K. A. Valiev, Nanotechnology **11**, 387 (2000); L. Fedichkin and A. Fedorov, Phys. Rev. A **69**, 032311 (2004).
[13] J. Kempe, D. Bacon, D. A. Lidar, and K. B. Whaley, Phys. Rev. A **63**, 042307 (2001).
[14] T. Brandes and T. Vorrath, Phys. Rev. B **66**, 075341 (2002).
[15] S. Vorojtsov, E. R. Mucciolo, and H. U. Baranger, Phys. Rev. B **71**, 205322 (2005).
[16] Z.-J. Wu, K.-D. Zhu, X.-Z. Yuan, Y.-W. Jiang, and H. Zheng, Phys. Rev. B **71**, 205323 (2005).
[17] V. N. Stavrou and X. Hu, Phys. Rev. B **72**, 075362 (2005).
[18] D. K. L. Oi, S. G. Schirmer, A. D. Greentree, and T. M. Stace, Phys. Rev. B **72**, 075348 (2005).
[19] M. Thorwart, J. Eckel, and E. R. Mucciolo, Phys. Rev. B **72**, 235320 (2005).
[20] M. J. Storcz, U. Hartmann, S. Kohler, and F. K. Wilhelm, Phys. Rev. B **72**, 235321 (2005).
[21] U. Hohenester, Phys. Rev. B **74**, 161307(R) (2006).
[22] W. G. van der Wiel, S. De Franceschi, J. M. Elzerman, T. Fujisawa, S. Tarucha, and L. P. Kouwenhoven, Rev. Mod. Phys. **75**, 1 (2002).
[23] R. Feynman, R. B. Leighon, and M. L. Sands, *The Feynman Lectures on Physics, Commemorative Issue* (Addison-Wesley, Reading, MA, 1964), Vol. 2.
[24] G.-L. Ingold and Yu. V. Nazarov, in *Single Charge Tunneling*, NATO Advanced Studies Institute, Series B Vol. 294, edited by H. Grabert and M. H. Devoret (Plenum, New York, 1992), p. 21107.
[25] L. P. Kouwenhoven, C. M. Marcus, P. L. McEuen, S. Tarucha, R. M. Westervelt, and N. S. Wingreen, in *Electron Transport in Quantum Dots*, NATO Advanced Studies Institute Conference Proceedings, edited by L. P. Kouwenhoven, G. Schon, and L. L. Sohn (Kluwer, Dordrecht, 1997).
[26] R. Hanson, Ph.D. thesis, Delft University of Technology, 2005.
[27] N. W. Ashcroft and N. D. Mermin, *Solid State Physics* (Brooks Cole, USA, 1976).
[28] C. W. J. Beenakker and H. van Houten, *Solid State Physics*, edited by H. Ehrenreich and D. Turnbull (Academic Press, New York, 1991), Vol. 44, p. 228.
[29] J. B. Kycia, J. Chen, R. Therrien, Ç. Kurdak, K. L. Campman, A. C. Gossard, and J. Clarke, Phys. Rev. Lett. **87**, 017002 (2001).
[30] E. B. Rosa and F. W. Grover, *Formulas and Tables for the Calculation of Mutual and Self-Induction*, Bulletin of the Bureau of Standards, Vol. 8 (Washington, DC, USA, 1912), pp. 150–166, Sec. 8.
[31] C. W. J. Beenakker, Phys. Rev. B **44**, 1646 (1991).
[32] E. di Lorenzo, FASTCAP 2 Software, MIT Research Lab of Electronics, Cambridge, MA, 1992.
[33] U. Weiss, *Quantum Dissipative Systems* (World Scientific, Singapore, 1999), Sec. 21.5.2.
[34] Y. Makhlin, G. Schön, and A. Shnirman, in *New Directions in Mesoscopic Physics (Towards Nanoscience)*, edited by R. Fazio, V. F. Gantmakher, and Y. Imry (Kluwer, Dordrecht, 2003).
[35] F. Marquardt and V. A. Abalmassov, Phys. Rev. B **71**, 165325 (2005).
[36] D. Culcer, X. Hu, and S. Das Sarma, Appl. Phys. Lett. **95**, 073102 (2009).
[37] H. Ribeiro, J. Petta, and G. Burkard, arXiv:1002.4630 (unpublished).
[38] M. Hentschel, D. C. B. Valente, E. R. Mucciolo, and H. U. Baranger, Phys. Rev. B **76**, 235309 (2007).
[39] B. Abel and F. Marquardt, Phys. Rev. B **78**, 201302(R) (2008).
[40] I. V. Yurkevich, J. Baldwin, I. V. Lerner, and B. L. Altshuler, Phys. Rev. B **81**, 121305(R) (2010).